Black holes in a new relativistic theory for modified Newtonian dynamics

Candidate 8257V,[1] W. E. V. Barker,[1,2] and A. Durakovic[3,4]

[1]*Cavendish Laboratory, JJ Thomson Avenue, Cambridge CB3 0HE, UK*

[2]*Kavli Institute for Cosmology, Madingley Road, Cambridge CB3 0HA, UK*

[3]*Institute of Physics of the Czech Academy of Sciences, Na Slovance 1999/2, Prague 182 000, Czechia*

[4]*Observatoire Astronomique de Strasbourg, UMR 7550, F-67000 Strasbourg, France*

Dark matter provides an explanation for multiple independent lines of astrophysical observations, but no corresponding particle signature has yet been detected, motivating the formulation of alternatives to general relativity with dark matter. Modified Newtonian dynamics is a hypothesis that suggests better agreement with observations of galaxy dynamics compared to dark matter, but by itself it cannot account for other gravitational effects. In this project, we study the features of a novel theory of modified gravity which for the first time reproduces Modified Newtonian dynamics and also accounts for the main cosmological observables. We obtain the field equations of the theory and reduce them to a special case in order to study gravity from static spherically symmetric sources. We then study for the first time the presence of horizons in the theory, finding differences with general relativity.

PACS numbers: 04.50.Kd

I. INTRODUCTION

Einstein's theory of general relavity (GR) has been greatly successful in its explanations for multiple physical phenomena. The theory first found acceptance because it provided a solution to the long-standing discrepancy in the apsidal precession of Mercury's orbit [1]. In the hundred years after it was postulated, its predictions of gravitational redshift [2], gravitational lensing [3], orbital decay in binary systems [4], black holes [5, 6], and gravitational waves [7] have all found observational confirmation.

However, if gravity is to be governed by Einstein's field equations, many phenomena in the Universe cannot be explained solely by its observable matter contents. The first example of this comes from galaxy rotation curves [8–10]. It is observed that the rotational velocity of gas and dust in spiral galaxies initially rises outwards from the centre, but at large enough distances it settles to a constant value. This shape of the rotation curves does not correspond to the observed mass distribution of the galaxies, requiring a correction, as will be outlined later in Eq. (4).

Additionally, in galaxy clusters, velocity dispersion measurements [11] allow for mass estimates using the virial theorem, which relates time-averaged kinetic energy T and potential energy U,

$$\langle T\rangle = -\frac{1}{2}\langle U\rangle. \tag{1}$$

The resulting values greatly exceed the masses due to observable (baryonic) matter. A deficit of mass has been noted from the velocity dispersion in individual elliptical galaxies as well [12]. A similar issue is found from gravitational lensing data [13]. The deflection of background light by galaxy clusters is significantly more than expected if the cluster mass was entirely due to baryons. The lensing in colliding galaxy clusters also does not follow the gas which permeates the clusters, but is instead most prominent in regions with little baryonic matter [14].

Finally, there are also challenges to structure formation in the Universe. In the high temperature early Universe, baryonic matter and radiation are coupled. Photon pressure and diffusion have a damping effect on the photon gas, and any perturbations in the fluid will oscillate rather than grow. This does not allow for the formation of overdensities that can act as gravitational wells after matter and radiation decouple, which would set off the formation of galaxies [15, 16]. Overdensities can grow only if the clumping of matter due to gravitiational attraction is not opposed by the pressure of the fluid.

These issues can be addressed by positing the presence of a type of matter that does not couple to anything except for gravity, called 'dark matter'. Because it addresses data from many independent avenues, dark matter has become the preferred hypothesis for explaining them. As of yet, no particle signature for dark matter has been detected despite significant efforts [17], motivating the alternative approach of seeking modified theories of gravity [18].

One important phenomenologically motivated theory in this class is modified Newtonian dynamics (MOND) [19], in which the acceleration $\mathbf{a}$ is given not by the usual Newtonian law $\mathbf{a}_\mathrm{N} = -\frac{GM}{r^2}\hat{\mathbf{r}}$, but is instead set by

$$\mathbf{a}\mu\left(\frac{|\mathbf{a}|}{a_0}\right) = -\frac{GM}{r^2}\hat{\mathbf{r}} \tag{2}$$

for circular orbits. Here $a_0 \sim 10^{-10}\,\mathrm{m/s^2}$ is a constant, and μ is a function which interpolates so that $\mu(x) \to x$ at $x \ll 1$ and $\mu(x) \to 1$ at $x \gg 1$. One possible example is

$$\mu(x) = \frac{x}{x+1}, \tag{3}$$

but the exact form of the function is inferred from observations [20, 21]. At low accelerations Eq. (2) reduces to

$$|\mathbf{a}| = \sqrt{|\mathbf{a}_\mathrm{N}|}\sqrt{a_0} = \frac{\sqrt{GMa_0}}{r}, \tag{4}$$

whereby the observed acceleration is the square root of the Newtonian expectation for the acceleration. This $a \propto 1/r$ be-

haviour leads to a constant rotation velocity v in galaxies, since for circular motion

$$a = \frac{v^2}{r}. \tag{5}$$

As can be seen from Eqs. (4) and (5), MOND behaviour recovers the empirircal baryonic Tully–Fisher relation $M \propto v^4$ for the baryonic mass [22]. This is a nontrivial observation, because if there is dark matter which influences rotational velocities significantly, the *baryonic* mass is not expected to correlate tightly with v since the dark matter mass distribution does not follow that of the baryonic mass.

The local correlation between baryonic surface density and kinematics in galaxies [23] is also explained better by MOND than by dark matter for the same reason. If there is a dominant dark matter component, the changes in rotation velocity are not predicted to keep to the baryonic surface density variations. The similar correspondence between local features in the luminosity profile and kinematics ('Renzo's rule') [24] also indicates that galaxy mass correlates to primarily baryonic matter. These and other dynamical properties have been generalised to a radial acceleration relation [25] that does not involve dark matter.

In addition, the theory predicts an 'external field effect', which is supported by observations [26] — the internal dynamics of galaxies will be influenced by other surrounding galaxies much more than anticipated in a Newtonian $\sim 1/r^2$ regime with dark matter.

The acceleration law in Eq. (2) does not naively respect conservation of momentum, as can be seen in the example of two interacting point masses $m \neq M$. There, we have

$$m|\mathbf{a_m}|\mu\left(\frac{|\mathbf{a_m}|}{a_0}\right) = \frac{GMm}{r^2} = M|\mathbf{a_M}|\mu\left(\frac{|\mathbf{a_M}|}{a_0}\right), \tag{6}$$

and if Newton's third law of motion holds, $m|\mathbf{a_m}| = M|\mathbf{a_M}|$ implies $\mu\left(\frac{|\mathbf{a_m}|}{a_0}\right) = \mu\left(\frac{|\mathbf{a_M}|}{a_0}\right)$, which cannot be true for different accelerations and a nonconstant interpolation function. This motivates reframing MOND in terms of an action principle, as this ensures that conservation laws are respected. Such a formulation is also more convenient for imposing symmetries and couplings between the fields in the theory. Milgrom and Bekenstein later formulated MOND through the action [27]

$$S_{\text{AQUAL}} \equiv -\int \mathrm{d}^3x \left(\rho\Phi + \frac{1}{8\pi G}a_0^2\mathcal{F}\left(\frac{|\vec{\nabla}\Phi|^2}{a_0^2}\right)\right), \tag{7}$$

which is the integral over space of a Lagrangian density that depends on the matter density ρ and the gravitational potential Φ. The interpolation function in this case is defined through the function $\mathcal{F}$ as $\mu(x) = \frac{\mathrm{d}\mathcal{F}(x^2)}{\mathrm{d}x}$. Extremising the action in Eq. (7) with the Euler–Lagrange equations leads to a modified Poisson equation,

$$\nabla \cdot \left(\mu\left(\frac{|\nabla\Phi|}{a_0}\right)\nabla\Phi\right) = 4\pi G\rho. \tag{8}$$

The acceleration is found with $\mathbf{a} = -\nabla\Phi$, whereby Eq. (8) reduces to Eq. (2) in the case of circular orbits due to a spherically symmetric mass distribution.

MOND is a nonrelativistic theory and hence it cannot immediately make predictions on cosmology [28] — the theory, for example, does not include a description of radiation, which dominates in the early Universe. MOND's assumptions also do not agree with galaxy cluster observations [14, 29]. The success of MOND for galactic dynamics, however, has prompted a search for generalised relativistic theories which recover MOND behaviour in the appropriate limit, but also match other observations (such as lensing, cluster dynamics, and cosmological data) without the need for dark matter. The action would have to incorporate a metric tensor to obey the Einstein equivalence principle [30]. If we are to deviate from GR, then, Lovelock's theorem either requires the action to be non-local, or to have additional fields apart from the metric [31]. Many theories with tensor fields of different rank have been constructed [18], though the couplings between the fields require adjustment to match GR in circumstances where it has been well-tested [32].

Past theories leading to MOND effects (e.g. [33–35]) have been rejected due to disagreement with data on gravitational wave polarisation and speed [36] or cosmological observables such as the cosmic microwave background (CMB) and the matter power spectrum (MPS) [16]. Here we make a digression to elaborate on why it is particularly difficult to account for the CMB and the MPS.

The CMB is the detected flux from photons emitted upon the recombination of free electrons and protons at redshift $z \simeq 1100$. This is the earliest observable radiation in the Universe, as before the recombination epoch, the absorption and reemission by the free baryons renders the Universe opaque to radiation. The CMB signal on the sky is standardly represented using a basis of spherical harmonic functions of different order ℓ. The $\ell = 0$ signal corresponds to a blackbody electromagnetic spectrum of mean temperature $T = 2.73\,\mathrm{K}$, but components with $\ell \geq 2$ reveal fine differences, with temperature anisotropies $\Delta T/T \sim 10^{-5}$ [37]. The dependence of anisotropy on ℓ, represented as an angular power spectrum, turns out to be related to the imprint of physical structure at recombination (specifically, information on the then-favoured length scales for structure in the Universe). This structure is modified from its initial form to the current day, where it can be measured and represented as the MPS. This evolution is standardly treated with cosmological perturbation theory on three fluids — baryonic matter, dark matter, and radiation. The relative height of the peaks in the CMB angular power spectrum and the shape of the peak in the MPS will then reflect the relative abundance of dark matter to baryons. Adding fields apart from the metric in a theory provides more degrees of freedom. Those will interact with baryonic matter and radiation in a complicated manner that will reflect on the CMB and the MPS. Relativistic MOND theories have had some success in reprodcing the CMB [34], but no match with the MPS has previously been achieved.

Recently, a new model which can match the cosmological

constraints has been proposed by Skordis and Zośnik [38], called 'Aether-Scalar-Tensor' (AeST). Like Bekenstein's TeVeS [34], it involves a scalar field ϕ and a vector field A^μ in addition to the metric $g_{\mu\nu}$. The vector field is chosen to be unit-timelike,

$$g_{\mu\nu}A^\mu A^\nu = -1, \tag{9}$$

giving it a directionality which sets a preferred frame and departs from the strong equivalence principle. The theory reproduces the cosmic microwave background (CMB) as shown on Fig. 1, as well as the matter power spectrum, shown on Fig. 2. It also provides the correct gravitational lensing phenomenology without dark matter. The existence of black hole-like behaviour in the theory has not yet been confirmed, and a negative result would effectively falsify it. The aim of this project is to derive the AeST field equations in the static spherically symmetric case, and then use them to check numerically for black hole solutions. There has been no previously published work on these topics, and the contributions that follow are original.

The structure of the project report is as follows: In Section II, we will outline how the field equations in AeST can be obtained from the action of the theory. In Section III, we will detail how those equations are reduced to the spherically symmetric case. Then, Section IV covers the numerical solution of the equations, the interpretation of the results, and directions for further work. Conclusions are presented in Section V. Appendices follow.

Throughout this report we will work in natural units such that $c = 1$, and we will use the East Coast $(-,+,+,+)$ convention for the metric signature. Parentheses '()' and brackets '[]' will be used in index notation to respectively indicate tensor symmetrisation and antisymmetrisation.

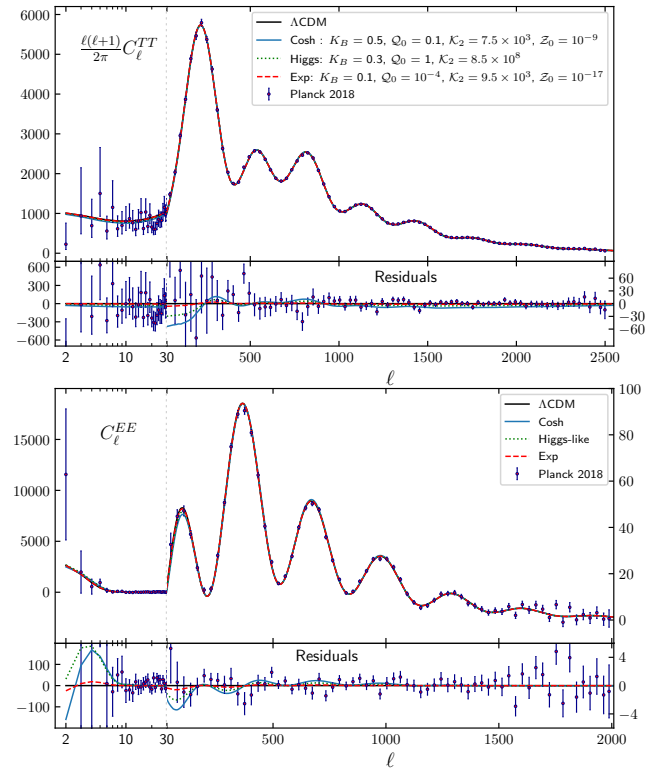

FIG. 1. CMB angular power spectra for temperature (top) and E-mode polarisation[a] (bottom), based on data from the Planck survey [16]. The x-axis stands for multipole numbers, with smaller ℓ equivalent to larger angular scales. The y-axis gives magnitudes in arbitrary units. Fits are shown for the standard Lambda cold dark matter model (ΛCDM) and for AeST. The fits for AeST correspond to three different choices of parameter values (K_B, $\mathcal{K}_2$, $\mathcal{Q}_0$[Mpc^{-1}], $\mathcal{Z}_0$[Mpc^{-1}]) and functions $\mathcal{F}$ in the action. Residuals are given with respect to ΛCDM data. From [38].

[a] This relates to anistropy in Thomson scattering of photons by free charged particles instead of anisotropy in temperature.

II. FIELD EQUATIONS

A. The AeST action

We will first introduce the Einstein–Hilbert action for general relativity, and describe how additional terms can be added to give the AeST action. The GR action incorporates the determinant of the metric, $g \equiv \det g_{\mu\nu}$, and the Ricci scalar R, which carries information about the curvature. The Ricci scalar R is defined from the Ricci tensor $R_{\mu\nu}$, the Riemann tensor $R_{\mu\nu\rho}{}^\sigma$, and the metric connection $\Gamma^\rho_{\mu\nu}$ through

$$\Gamma^\rho_{\mu\nu} \equiv \frac{1}{2}g^{\rho\kappa}(\partial_\mu g_{\nu\kappa} + \partial_\nu g_{\mu\kappa} - \partial_\kappa g_{\mu\nu}), \tag{10a}$$

$$R_{\mu\nu\rho}{}^\sigma \equiv -\partial_\mu\Gamma^\sigma_{\nu\rho} + \partial_\nu\Gamma^\sigma_{\mu\rho} + \Gamma^\kappa_{\mu\rho}\Gamma^\sigma_{\nu\kappa} - \Gamma^\kappa_{\nu\rho}\Gamma^\sigma_{\mu\kappa}, \tag{10b}$$

$$R_{\mu\nu} \equiv R_{\rho\mu\nu}{}^\rho, \tag{10c}$$

$$R \equiv g^{\mu\nu}R_{\mu\nu}. \tag{10d}$$

The total Einstein–Hilbert action, when split up into gravitational and matter parts $S_{\rm EH} \equiv S_{\rm g} + S_{\rm m}$, is given by

$$S_{\rm EH} \equiv \int {\rm d}^4x \left(\frac{\sqrt{-g}}{16\pi G}R\right) + S_{\rm m}. \tag{11}$$

Representing the matter action with a Lagrangian, $S_{\rm m} \equiv \int {\rm d}^4x\,\mathcal{L}_{\rm m}$, we define the stress-energy tensor

$$T_{\mu\nu} \equiv \frac{-2}{\sqrt{-g}}\frac{\delta\mathcal{L}_{\rm m}}{\delta g^{\mu\nu}}. \tag{12}$$

We further define the Einstein tensor as

$$G_{\mu\nu} \equiv R_{\mu\nu} - \frac{1}{2}g_{\mu\nu}R. \tag{13}$$

Varying Eq. (11) with respect to the metric $g_{\mu\nu}$, we can obtain Einstein's equations, which relate the curvature of spacetime to the matter distribution:

$$G_{\mu\nu} = 8\pi G T_{\mu\nu}. \tag{14}$$

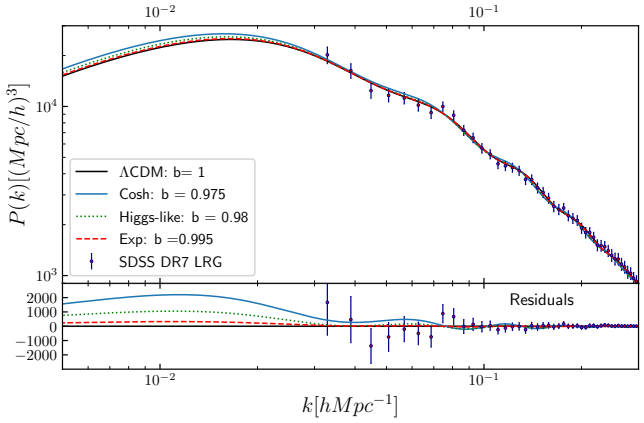

FIG. 2. The matter power spectrum $P(k)$ with respect to wavenumbers k, based on data from the Sloan Digital Sky Survey data on luminous red galaxies (LRGs) [39]. Fits are shown for the standard Lambda cold dark matter model (ΛCDM) and for AeST. The fits for AeST correspond to three different choices of functions $\mathcal{F}$ in the action, with different bias parameters b. Residuals are given with respect to ΛCDM data. From [38].

The unit-timelike vector field A^μ and the scalar field ϕ allow us to form other terms in addition to R, all according to the definitions given in Eq. (15). To avoid unbounded Hamiltonians, we will choose the terms in the action to scale as even powers of the fields. For non-interacting (single-field) terms, we will limit ourselves to a term $\sim F^{\mu\nu}F_{\mu\nu}$, which is the unique ghost-free vector kinetic structure [40]. When variations are taken, this will produce a term that is linear in the gradient of the vector field.

Now we consider interacting terms. From the vector field, we introduce the divergence J and the projected vector gradient J_μ. The vector field can then interact with the scalar field through a term $2(2-K_B)J^\mu\nabla_\mu\phi$, where a coupling constant K_B in the range $0 < K_B < 2$ adjusts the magnitude of the interaction. To join the metric with the two other fields, we define the induced metric $q_{\mu\nu}$. We then introduce terms $\mathcal{Q}$ and $\mathcal{Y}$, which represent the parallel and the perpendicular components of the scalar gradient $\nabla_\mu\phi$ with respect to the vector field A^μ:

$$F_{\mu\nu} \equiv 2\nabla_{[\mu}A_{\nu]}, \tag{15a}$$
$$J \equiv \nabla_\mu A^\mu, \tag{15b}$$
$$J_\mu \equiv A^\nu\nabla_\nu A_\mu, \tag{15c}$$
$$q_{\mu\nu} \equiv g_{\mu\nu} + A_\mu A_\nu, \tag{15d}$$
$$\mathcal{Q} \equiv A^\mu\nabla_\mu\phi, \tag{15e}$$
$$\mathcal{Y} \equiv q^{\mu\nu}\nabla_\mu\phi\nabla_\nu\phi. \tag{15f}$$

The AeST action $S_{\rm AeST}$ introduces $\tilde{G}$, a bare gravitational constant which need not correspond to the Newtonian gravitational constant G we measure in a large (i.e. Newtonian, $a \gg a_0$) acceleration regime. The action, again represented in gravitational and matter parts $S_{\rm AeST} \equiv S_{\rm g} + S_{\rm m}$, is then

$$S_{\rm AeST} \equiv \int {\rm d}^4x\,\frac{\sqrt{-g}}{16\pi\tilde{G}}\Big(R - \frac{K_B}{2}F^{\mu\nu}F_{\mu\nu} + 2(2-K_B)J^\mu\nabla_\mu\phi - (2-K_B)\mathcal{Y} - \mathcal{F}(\mathcal{Y},\mathcal{Q}) - \lambda(A^\mu A_\mu + 1)\Big) + S_{\rm m}[g]. \tag{16}$$

We note that the action includes λ as a Lagrange multiplier field which imposes the unit-timelike constraint on A^μ. More specifically, λ acts as an auxiliary field, and extremising $S_{\rm AeST}$ with respect to it yields Eq. (9) as an additional constraint equation,

$$\frac{\delta S_{\rm AeST}}{\delta\lambda} = A^\mu A_\mu + 1 = 0. \tag{17}$$

In Eq. (16), $\mathcal{F}$ is a free function of $\mathcal{Y}$ and $\mathcal{Q}$. There are many possible terms that $\mathcal{F}$ can incorporate, and we will specify the choice that we work with in Section II C. Accordingly, the field equations will now be given without explicitly specifying the form of $\mathcal{F}$, instead using $\mathcal{F}_\mathcal{Y}$ and $\mathcal{F}_\mathcal{Q}$ to respectively indicate its partial derivatives with respect to $\mathcal{Y}$ and $\mathcal{Q}$.

B. Derivation of the field equations

The field equations can be found by extremising the Lagrangian density in the action $S \equiv \int {\rm d}^4x\,\mathcal{L}$ with respect to any field q^i,

$$\frac{\delta\mathcal{L}}{\delta q^i} = 0. \tag{18}$$

The action in Eq. (16) has no algebraic dependence on ϕ, implying

$$\nabla_\mu\left(\frac{\partial\mathcal{L}}{\partial(\nabla_\mu\phi)}\right) = 0. \tag{19}$$

Extremising for ϕ then gives the scalar equation

$$\nabla_\mu\left((2-K_B)J^\mu - (2-K_B+\mathcal{F}_\mathcal{Y})D^\mu\phi - \frac{1}{2}\mathcal{F}_\mathcal{Q}A^\mu\right) = 0, \tag{20}$$

where $D^\mu \equiv q^{\mu\nu}\nabla_\nu$. The procedure can be repeated for A^μ. Accounting for the antisymmetricity of $F_{\mu\nu}$ and contracting the intermediate result,

$$\nabla_\nu\left(-\frac{K_B}{2}(4F^\nu{}_\mu) + 2(2-K_B)A^\nu\nabla_\mu\phi\right) = 2(2-K_B)\nabla_\mu A^\nu\nabla_\nu\phi - 2(2-K_B)A^\nu\nabla_\nu\phi\nabla_\mu\phi - 2\mathcal{F}_\mathcal{Y}A^\nu\nabla_\nu\phi\nabla_\mu\phi - \mathcal{F}_\mathcal{Q}\nabla_\mu\phi - 2\lambda A_\mu, \tag{21}$$

with the induced metric $q^\mu{}_\sigma$ to eliminate the Lagrange multiplier using the timelike constraint (Eq. (9)), we obtain the vector equations

$$K_B q^\rho{}_\mu \nabla_\nu F^\nu{}_\rho + (2-K_B)\nabla^\nu\phi D_\mu A_\nu - \left((2-K_B+\mathcal{F}_\mathcal{Y})\mathcal{Q} + \frac{1}{2}\mathcal{F}_\mathcal{Q} + (2-K_B)J\right) D_\mu\phi - (2-K_B)D_\mu\mathcal{Q} = 0, \quad (22)$$

after relabelling the indices. Furthermore, multiplying Eq. (21) by A^μ allows the value of the Lagrange multiplier to be algebraically determined,

$$\lambda = \left(2-K_B\right)\mathcal{Q}J + \left(2-K_B+\mathcal{F}_\mathcal{Y}\right)\mathcal{Q}^2 - \left(2-K_B\right)\nabla^\nu\phi J_\nu + \left(2-K_B\right)A^\mu A^\nu \nabla_\nu\nabla_\mu\phi + \frac{1}{2}\mathcal{Q}\mathcal{F}_\mathcal{Q} - K_B A^\mu \nabla_\nu F^\nu_\mu, \quad (23)$$

and this result can be substituted when taking variations with respect to the metric $g^{\mu\nu}$.

The variations of Eq. (16) with respect to the metric are significantly more involved, and it is prudent to verify the tensor field equations,

$$\begin{aligned} G_{\mu\nu} = {} & 8\pi G T_{\mu\nu} + (2-K_B+\mathcal{F}_\mathcal{Y})D_\mu\phi D_\nu\phi + \mathcal{F}_\mathcal{Q} D_{(\mu}\phi A_{\nu)} - 2(2-K_B)(\nabla_\rho\phi)\left(A_{(\mu}\nabla_{\nu)}A^\rho - A_{(\mu}\nabla^\rho A_{\nu)}\right) \\ & - 2(2-K_B)\nabla_{(\mu}\phi J_{\nu)} - K_B F^\rho{}_{(\mu} F_{\nu)\rho} + \frac{1}{2}\left(-\frac{K_B}{2}F_{\alpha\beta}F^{\alpha\beta} + 2(2-K_B)J^\rho\nabla_\rho\phi - (2-K_B)\mathcal{Y} - \mathcal{F}\right) g_{\mu\nu} \\ & + \left((2-K_B)\left(q^\lambda{}_\rho \nabla_\lambda\nabla^\rho\phi + J\mathcal{Q} - D^\rho\phi J_\rho\right) - K_B A^\rho \nabla_\lambda F^\lambda{}_\rho - \frac{1}{2}\mathcal{Q}\mathcal{F}_\mathcal{Q}\right) A_\mu A_\nu, \end{aligned} \quad (24)$$

with the assistance of computer algebra. For this purpose, the tensor algebra suite `xAct` was used to check our expression [41, 42]. The relevant code is presented in Appendix A. It was confirmed that the tensor equations indeed take the form in Eq. (24).

C. Choice of free function and the weak field limit

For our work in Sections III and IV, we will use a free function of the form

$$\mathcal{F}(\mathcal{Y},\mathcal{Q}) \equiv \mathcal{F}_{20}(\mathcal{Q}-\mathcal{Q}_0)^2 + \mathcal{J}(\mathcal{Y}), \quad (25)$$

where in the large and small acceleration regimes $\mathcal{J}(\mathcal{Y})$ respectively reduces to

$$\mathcal{J}(\mathcal{Y}) = \begin{cases} (2-K_B)\lambda_s\mathcal{Y}, & |\nabla\phi| \gg a_0, \\ \frac{2\lambda_s}{3(1+\lambda_s)a_0}\mathcal{Y}^{3/2}, & |\nabla\phi| \ll a_0. \end{cases} \quad (26)$$

The parameter λ_s is related to screening, and the bare $\tilde{G}$ is adjusted in the Newtonian regime [43] to give the gravitational constant

$$G \equiv \frac{1+\lambda_s}{\lambda_s}\frac{2\tilde{G}}{2-K_B} = 6.674\times10^{-11}\,\mathrm{kg}^{-1}\,\mathrm{m}^3\,\mathrm{s}^{-2}. \quad (27)$$

When cosmological evolution is relevant, other terms may be added to $\mathcal{F}$, such as a 'Higgs-like' term $\sim \frac{1}{4\mathcal{Q}_0^2}(\mathcal{Q}^2-\mathcal{Q}_0^2)^2$ which recovers the CMB. For our analysis, the terms in Eq. (25) are sufficient.

In the first term of Eq. (25), $\mathcal{Q}_0$ is defined to be constant. When $\mathcal{Q}=\mathcal{Q}_0$, the fields provide a homogeneous background. In the special case $\mathcal{Q}=\mathcal{Q}_0$, the free function $\mathcal{F}(\mathcal{Y},\mathcal{Q})$ is minimised, hence a Taylor expansion of the free function in $\mathcal{Q}$ about $\mathcal{Q}_0$ will have a zero first-order term. The first physically meaningful term is of second order, with the respective coefficient $\mathcal{F}_{20}$. The role of this term is to provide a cosmological dark matter density.

For a homogeneous background, there is no curvature and the metric is Minkowski, $g_{\mu\nu}=\eta_{\mu\nu}=\mathrm{diag}(-1,1,1,1)$. The vector field cannot have a preferred direction in space, leading to $A^\mu=(1,0,0,0)$. Therefore, in that case $\mathcal{Q}=A^\mu\nabla_\mu\phi=\dot{\phi}\equiv\mathcal{Q}_0$, which gives $\phi=\mathcal{Q}_0 t$.

For the scalar field, we can then isolate a part which provides the background,

$$\phi(r,t) \equiv \mathcal{Q}_0 t + \varphi(r,t), \quad (28)$$

and any physical effects superposed onto the background are then associated with $\varphi(r,t)$.

The second term of Eq. (25) produces MOND behaviour at $|\nabla\phi| \ll a_0$. For this to be made clear, we will consider the field equations in weak field limit of the theory. In this limit, the background in $\phi(r,t)$ dominates as the vector field projects entirely along time, hence

$$\mathcal{Q} \equiv A^\mu\nabla_\mu\phi \to \dot{\phi}. \quad (29)$$

Additionally, gradients in time become negligible to spatial gradients, resulting in

$$\mathcal{Y} \equiv q^{\mu\nu}\nabla_\mu\phi\nabla_\nu\phi \to |\nabla\phi|^2 \to |\nabla\varphi|^2. \quad (30)$$

For our purposes the screening term λ_s will tend to infinity in the weak field limit — it will not suppress $\mathcal{J}(\mathcal{Y})$ and will not

be considered explicitly onwards. In a weak field regime with gravitational potential Φ, the invariant interval [44] is

$$\mathrm{d}s^2 = -(1+2\Phi)\,\mathrm{d}t^2 + (1-2\Phi)(\mathrm{d}x^2+\mathrm{d}y^2+\mathrm{d}z^2), \quad (31)$$

with the metric perturbations given by

$$h_{\mu\nu} = (-2\Phi)\,\mathrm{diag}(1,1,1,1). \quad (32)$$

Then, using Eqs. (29) to (31), the weak field expansion of Eq. (20) is found to be

$$\nabla\Phi = \left(1 + \frac{\mathrm{d}\mathcal{J}}{\mathrm{d}\mathcal{Y}}\Big|_{\mathcal{Y}=|\nabla\varphi|^2}\right)\nabla\varphi. \quad (33)$$

For the $\mathcal{J}(\mathcal{Y})$ choice of Eq. (26) without screening we find,

$$1 + \frac{\mathrm{d}\mathcal{J}}{\mathrm{d}\mathcal{Y}}\Big|_{\mathcal{Y}=|\nabla\varphi|^2} = 1 + \frac{|\nabla\varphi|}{a_0}, \quad (34)$$

and taking the magnitudes in Eq. (33), we obtain

$$\frac{|\nabla\Phi|}{a_0} = \left(1+\frac{|\nabla\varphi|}{a_0}\right)\left(\frac{|\nabla\varphi|}{a_0}\right). \quad (35)$$

We solve this in terms of the scalar field, taking the physical root of the quadratic equation:

$$|\nabla\varphi| = \left(\frac{-1+\sqrt{1+4\frac{|\nabla\Phi|}{a_0}}}{2\frac{|\nabla\Phi|}{a_0}}\right)|\nabla\Phi|. \quad (36)$$

Because the acceleration will be directed along the gradient of the scalar field, it follows that

$$\nabla\varphi = \left(\frac{-1+\sqrt{1+4\frac{|\nabla\Phi|}{a_0}}}{2\frac{|\nabla\Phi|}{a_0}}\right)\nabla\Phi. \quad (37)$$

Denoting $x \equiv |\nabla\Phi|/a_0$ and taking the divergence of Eq. (37),

$$\nabla^2\varphi = \nabla\cdot\left(\frac{-1+\sqrt{1+4x}}{2x}\nabla\Phi\right). \quad (38)$$

Now, using Eqs. (29) and (30) again, we can derive the weak field expansion of the 00-component of Eq. (24):

$$\nabla^2\Phi - \nabla^2\varphi = 4\pi\hat{G}\rho - m^2\Phi, \quad (39)$$

where we have introduced the notation

$$\hat{G} \equiv \frac{2\tilde{G}}{2-K_B}, \quad m^2 \equiv \frac{\mathcal{F}_{20}\mathcal{Q}_0^2}{2-K_B}. \quad (40)$$

Substituting Eq. (37) into Eq. (39) yields

$$\nabla\cdot\left(\frac{1+2x-\sqrt{1+4x}}{2x}\nabla\Phi\right) = 4\pi\hat{G}\rho - m^2\Phi, \quad (41)$$

or equivalently,

$$\nabla\cdot\left(\frac{\sqrt{1+4x}-1}{\sqrt{1+4x}+1}\nabla\Phi\right) = 4\pi\hat{G}\rho - m^2\Phi. \quad (42)$$

This result is identical to Eq. (8) for an interpolation function

$$\mu(x) = \frac{\sqrt{1+4x}-1}{\sqrt{1+4x}+1}. \quad (43)$$

Eq. (43) satisfies $\mu(x) \to x$ at $x \ll 1$ and $\mu(x) \to 1$ at $x \gg 1$, thus accounting for Newtonian and MOND-like behaviour.

In AeST, there is an additional term $m^2\Phi$, which will dominate the dynamics below another acceleration scale $a_m \ll a_0$. In this regime, the potential from a point source will have oscillatory behaviour [38]. The theory then has the following regimes depending on the local gravitational acceleration:

(i) A μ-dominated regime for $a \sim a_m$, where a oscillates with the distance from a point source.

(ii) A MOND regime for $a \sim a_0$, where $a \sim 1/r$.

(iii) A Newtonian regime for $a \gg a_0$, but still well into the weak field approximation, where $a \sim 1/r^2$.

(iv) A strong-field regime, which has not been studied, and is in the scope of this work.

III. SPHERICALLY SYMMETRIC REDUCTION

We will now consider the special case of a static compact spherically symmetric source in AeST, working in a spherical polar coordinate system (t, r, θ, ψ). This symmetry of the source is reflected in the form of the fields. For the space part of the metric, the radial coordinate is privileged over the angular coordinates, and it therefore incorporates the curvature while the angular coordinates retain Euclidean geometry. This is a Schwarzschild-like metric, where the diagonal form of the line element is

$$\mathrm{d}s^2 = -T(r)\,\mathrm{d}t^2 + R(r)\,\mathrm{d}r^2 + r^2\,\mathrm{d}\Omega^2\,. \quad (44)$$

The coefficients can be taken as positive, because outside any horizons they must allow for a reduction to a locally Lorentzian metric. To impose this, they are written as $T(r) \equiv e^{\mathcal{T}(r)}$ and $R(r) \equiv e^{\mathcal{R}(r)}$. The metric and its inverse are

$$g_{\mu\nu} = \begin{pmatrix} -e^{\mathcal{T}} & 0 & 0 & 0 \\ 0 & e^{\mathcal{R}} & 0 & 0 \\ 0 & 0 & r^2 & 0 \\ 0 & 0 & 0 & r^2\sin^2\theta \end{pmatrix}, \quad (45a)$$

$$g^{\mu\nu} = \begin{pmatrix} -e^{-\mathcal{T}} & 0 & 0 & 0 \\ 0 & e^{-\mathcal{R}} & 0 & 0 \\ 0 & 0 & r^{-2} & 0 \\ 0 & 0 & 0 & r^{-2}\sin^{-2}\theta \end{pmatrix}. \quad (45b)$$

The vector field A^μ can only point radially in space — its radial component will be denoted by $A(r)$, having assumed time

independence. The timelike constraint in Eq. (9) leads to

$$A^\mu = \left(\sqrt{e^{-\mathcal{T}}(e^{\mathcal{R}}(A)^2+1)},\ A,\ 0,\ 0\right), \tag{46a}$$

$$A_\mu = \left(\sqrt{e^{\mathcal{T}}(e^{\mathcal{R}}(A)^2+1)},\ e^{\mathcal{R}}A,\ 0,\ 0\right). \tag{46b}$$

The scalar field ϕ is allowed a time dependence provided that it does not explicitly manifest in the field equations. In Eq. (28), the time dependence for the background term remains, while $\varphi(r)$ represents the static source:

$$\phi(r,t) = \mathcal{Q}_0 t + \varphi(r). \tag{47}$$

The spherically symmetric equations follow by replacing the component values of Eqs. (45) to (47) into Eqs. (20), (22) and (24), taking the necessary covariant derivatives, and simplifying. This will eliminate the explicit time dependence from the background $\mathcal{Q}_0 t$. This procedure is again carried out through `xAct` with the component calculation package `xCoba`, the canonicalisation package `xPerm` [45], and the field theory package `xTras` [46].

A sample of the code for one equation is provided in Appendix B, and the resulting output is presented in Appendix C. In total, there are six second-order ordinary differential equations for the four dependent variables $\varphi(r)$, $A(r)$, $T(r)$, and $R(r)$[1]. They correspond to variations for ϕ, A^t, A^r, g^{tt}, g^{rr}, g^{tr}, and two of them will be redundant.

IV. BLACK HOLE SOLUTIONS

A. Initial conditions

We can now form a well-determined system of four differential equations with the four dependent variables, but it is further required to specify initial conditions to solve them numerically. This needs to be done at a distance from the source where it is known how the values of the fields relate to the local gravitational potential Φ. A distance with MOND behaviour will be chosen, in which case the analytic solution for the potential is

$$\Phi(r) = -\frac{GM}{r} - \sqrt{GMa_0}\ln\left(\frac{r}{r_0}\right), \tag{48}$$

with r_0 being an arbitrary constant. Because this is a weak field regime [44], the metric will be set by

$$T(r) = 1 + 2\Phi(r), \quad R(r) = 1 - 2\Phi(r), \tag{49}$$

from which we can read off

$$\mathcal{T} = \ln(1+2\Phi), \quad \mathcal{R} = \ln(1-2\Phi). \tag{50}$$

[1] There is a meaningful off-diagonal tensor equation because $q^{\mu\nu}$ gets off-diagonal contributions from $A^\mu A^\nu$.

For the vector field A^μ, there is a degree of freedom in the choice of the radial component A, provided that the time component is set to $\sqrt{e^{-\mathcal{T}}(e^{\mathcal{R}}(A)^2+1)}$ in accordance with the constrant in Eq. (9).

The scalar field is obtained by taking the gradient of the potential in Eq. (48), and then integrating (over distance) the deep-MOND limit of Eq. (37),

$$\frac{|\nabla\varphi|}{a_0} = \left(1 - \frac{|\nabla\Phi|}{a_0}\right)\left(\frac{|\nabla\Phi|}{a_0}\right). \tag{51}$$

Having established the weak field regime initial conditions, we must now ensure that the distance we are applying them at indeed corresponds to the MOND regime. For this purpose we require the distance scales which correspond to transitions between the regimes of the theory considered in Section II C. At the Newtonian–MOND transition distance $r_{\rm MOND}$ ('MOND radius'), the magnitudes of the MOND gravitational acceleration of Eq. (4) and the Newtonian acceleration match,

$$\frac{GM}{r_{\rm MOND}^2} \sim \frac{\sqrt{GMa_0}}{r_{\rm MOND}} \Rightarrow r_{\rm MOND} \sim \sqrt{\frac{GM}{a_0}}. \tag{52}$$

For the case of the MOND–m transition distance r_m ('m-radius'), only the MOND radius $r_{\rm MOND}$ and the quantity m may reflect on the distance scale. An involved calculation [47] yields

$$r_m \sim \left(\frac{r_{\rm MOND}}{m^2}\right)^{1/3}. \tag{53}$$

We additionally consider the Schwarzschild radius

$$r_{\rm s} = 2GM, \tag{54}$$

which corresponds to the horizon for static spherically symmetric black holes in GR. It also indicates a characteristic distance scale for the transition between the strong field regime and the Newtonian regime where acceleration scales as $\sim 1/r^2$.

It is necessary to impose well-separated regimes in our numerical solution for the potential, choosing the parameter values so that

$$r_{\rm g} \ll r_{\rm MOND} \ll r_m. \tag{55}$$

The initial conditions will then be set at a distance $r_{\rm W}$ between $r_{\rm MOND}$ and r_m.

B. A Tensor-Vector solution

We now examine a special case of AeST with only the metric and the vector field active. Firstly we will consider the instance where the radial component A of the vector field, as defined in Eq. (46), is constrained to be zero via the initial conditions of zero value and zero derivative at the distance $r_{\rm W}$. This choice is based on the expectation that in the weak field regime the vector field should maintain small components. Restricting A in this manner does not eliminate the time component

of the vector field, which will still vary with distance, as can be seen from taking the derivative of the unit-timelike constraint in Eq. (9). Nevertheless, this constitutes the simplest non-Schwarzschild phenomenology in AeST.

In this limit it is possible to eliminate the time component of the vector field $A^t(r)$ and the radial component of the metric $R(r)$ from the system of equations found in Section III, thereby obtaining a differential equation only in $T(r)$,

$$K_B r^2 (T')^3 + 8T^2(2T' + rT'') = 0. \tag{56}$$

If we additionally impose $K_B = 0$, AeST must reduce to general relativity. It can be verified that Eq. (56) then reduces as expected to a differential equation which is satisfied by the Schwarzschild solution in GR,

$$T(r) = 1 - \frac{r_g}{r}, \tag{57a}$$

$$R(r) = \left(1 - \frac{r_g}{r}\right)^{-1}. \tag{57b}$$

Following from Eq. (56), we can find *implicit* analytic solutions for $T(r)$, and through further substitutions, repeat this for $R(r)$. The solutions are presented in Appendix D.

For simplicity, we proceed to solve the system of equations numerically as outlined in Section IV A. We will now turn off the time component of the vector field as opposed to the radial component, but identical behaviour is expected in both cases. Plotting the result for $R(r)$, we can observe divergence $r \to r_g$. The AeST solution is compared to the Schwarzschild metric on Fig. 3, with the relative deviation displayed on Fig. 4.

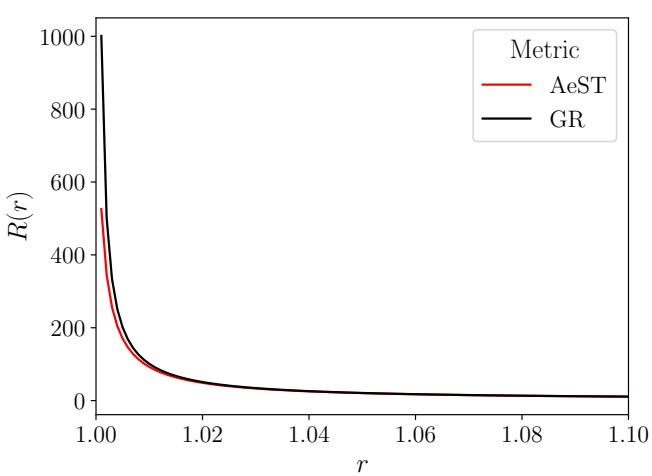

FIG. 3. Dependence of the metric $R(r)$ on distance r from the centre of the source (in units of Schwarzschild radii), plotted for general relativity and AeST with zero time component of the vector field. The AeST solution corresponds to a coupling $K_B = 1$ and a MOND radius $r_{\rm MOND} = 1000$.

To generalise our results, we also explore the form of the solutions under general initial conditions for the vector field at r_W. When increasing the time component $A^t(r_W)$, the numerical solution for the metric $R(r)$ is found to retain the horizon at r_g up to a value of $A^t(r_W) \approx 0.077$, which is well into

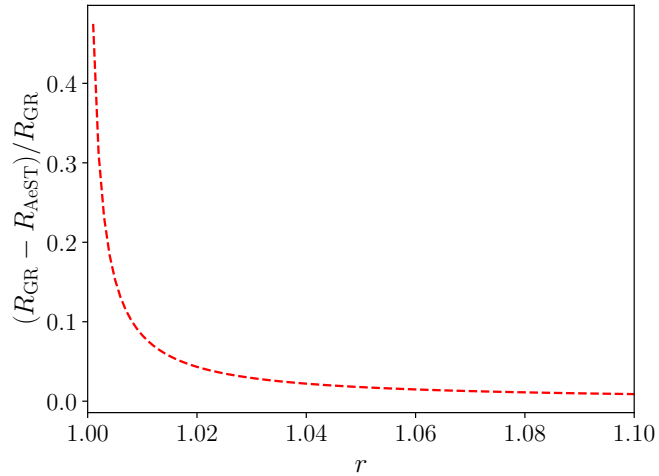

FIG. 4. Relative deviation of the AeST Tensor-Vector solution from the Schwarzschild solution for the radial component of the metric $R(r)$.

the regime of strong vector fields[2]. For larger values of the time component, the singularity smoothly transitions to a maximum, as shown on Fig. 5. The distance of the maximum from the centre of the source is observed to increase with $A^t(r_W)$, and its magnitude is found to simultaneously decay.

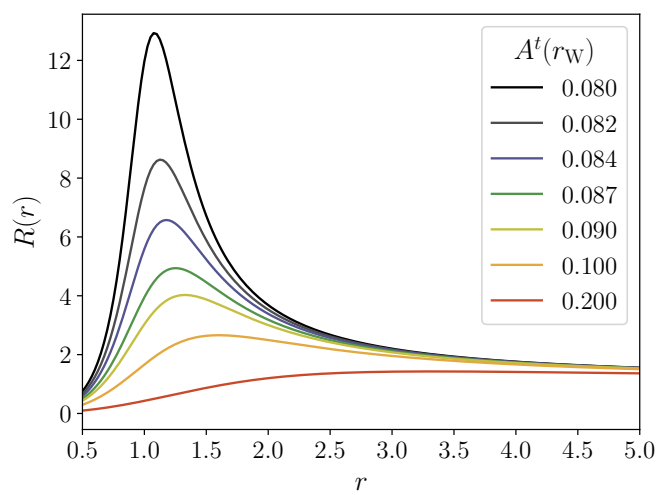

FIG. 5. Dependence of the metric $R(r)$ on the distance r from the centre of the source (in units of Schwarzschild radii). The plots are given for coupling $K_B = 1$, MOND radius $r_{\rm MOND} = 100$, and different initial conditions on the time component A^t of the vector field at a distance $r_W = 1000$. As $A^t(r_W)$ is increased beyond a critical value of 0.077, the singularity in the metric at $r = 1$ transitions to a maximum.

Due to the time constraints of the project, we have not studied black hole-like behaviour in the general scalar-vector-tensor

[2] For reference, the magnitude of the weak field metric perturbations $|h_{rr}|$ is $\sim 10^{-3}$ at a distance r_W.

case. Extending our numerical routines to the scalar field is a significant undertaking due to the complexity of the AeST field equations, particularly in terms of φ. The results obtained above pertain only to a special case of the theory, and general conclusions on the phenomenology of black hole solutions cannot be made freely. However, this project has provided valuable initial insights into the theory's characteristics near horizons, which will be explored in more detail in our further work.

V. CONCLUSIONS

The novel Aether-Scalar-Tensor model is the first theory that can reproduce Modified Newtonian dynamics and simultaneously account for cosmological data. We have studied the features of this theory, making multiple original contributions. Starting from the action of the theory, we derived the general field equations, verifying them with the help of computer algebra. We then obtained the form that these equations take for a static spherically symmetric source. These equations were finally used to examine black hole-like solutions in a regime without the scalar field, comparing with the standard solution in general relativity.

Future work in this direction will primarily focus on such solutions in the general case. Particular topics of interest include the potential presence of naked singularities and the potential instability of the static solutions that we found. Developments along those lines for the general theory will help us provide a meaningful interpretation of the physically interesting results outlined so far.

ACKNOWLEDGEMENTS

Candidate 8257V wishes to express their sincere gratitude to the project supervisors, William Barker and Amel Durakovic, for their invaluable support and advice throughout the year. The candidate also wishes to thank Will Handley and John Ellis for many helpful conversations. The supervisors W.E.V.B. and A.D. are grateful for the useful correspondence with Tom Zosnik and Costantinos Skordis.

[1] A. Einstein, Sitzungsberichte der Königlich Preussischen Akademie der Wissenschaften , 831 (1915).
[2] D. M. Popper, The Astrophysical Journal **120**, 316 (1954).
[3] F. W. Dyson, A. S. Eddington, and C. Davidson, Philosophical Transactions of the Royal Society of London. Series A, Containing Papers of a Mathematical or Physical Character **220**, 291 (1920).
[4] R. A. Hulse and J. H. Taylor, The Astrophysical Journal **195**, L51 (1975).
[5] B. L. Webster and P. Murdin, Nature **235**, 37 (1972).
[6] T. E. H. T. Collaboration, ApJ, 875, L1, 2019 (April 10) (2019), 10.3847/2041-8213/ab0ec7, arXiv:1906.11238 [astro-ph.GA].
[7] B. Abbott, Physical Review Letters **116**, 061102 (2016).
[8] V. C. Rubin and J. F. W. Kent, The Astrophysical Journal **159**, 379 (1970).
[9] V. C. Rubin, N. Thonnard, and J. F. W. Kent, The Astrophysical Journal **238**, 471 (1980).
[10] M. Persic, P. Salucci, and F. Stel, Monthly Notices of the Royal Astronomical Society **281**, 27 (1996).
[11] F. Zwicky, The Astrophysical Journal **86**, 217 (1937).
[12] S. M. Faber and R. E. Jackson, The Astrophysical Journal **204**, 668 (1976).
[13] A. N. Taylor, S. Dye, T. J. Broadhurst, N. Benitez, and E. van Kampen, The Astrophysical Journal **501**, 539 (1998).
[14] D. Clowe, M. Bradač, A. H. Gonzalez, M. Markevitch, S. W. Randall, C. Jones, and D. Zaritsky, The Astrophysical Journal **648**, L109 (2006).
[15] S. D. M. White and M. J. Rees, Monthly Notices of the Royal Astronomical Society **183**, 341 (1978).
[16] N. Aghanim et al., Astronomy & Astrophysics **641**, A6 (2020).
[17] J. Billard, M. Boulay, S. Cebrián, L. Covi, G. Fiorillo, A. Green, J. Kopp, B. Majorovits, K. Palladino, F. Petricca, L. Roszkowski, and M. Schumann, (2021), 10.48550/ARXIV.2104.07634.
[18] T. Clifton, P. G. Ferreira, A. Padilla, and C. Skordis, Physics Reports 513, 1 (2012), 1-189 (2011), 10.1016/j.physrep.2012.01.001, arXiv:1106.2476 [astro-ph.CO].
[19] M. Milgrom, The Astrophysical Journal **270**, 371 (1983).
[20] B. Famaey and J. Binney, Monthly Notices of the Royal Astronomical Society **363**, 603 (2005).
[21] G. Gentile, B. Famaey, and W. J. G. de Blok, Astronomy & Astrophysics **527**, A76 (2011).
[22] R. B. Tully and J. R. Fisher, Astronomy & Astrophysics **54**, 661 (1977).
[23] B. Famaey and S. McGaugh, 2012, Living Reviews in Relativity, 15, 10 (2011), 10.12942/lrr-2012-10, arXiv:1112.3960 [astro-ph.CO].
[24] R. Sancisi, (2003), 10.48550/ARXIV.ASTRO-PH/0311348.
[25] F. Lelli, S. S. McGaugh, J. M. Schombert, and M. S. Pawlowski, The Astrophysical Journal **836**, 152 (2017).
[26] K.-H. Chae, F. Lelli, H. Desmond, S. S. McGaugh, P. Li, and J. M. Schombert, The Astrophysical Journal **904**, 51 (2020).
[27] J. Bekenstein and M. Milgrom, The Astrophysical Journal **286**, 7 (1984).
[28] D. Scott, M. White, J. D. Cohn, and E. Pierpaoli, (2001), arXiv:astro-ph/0104435 [astro-ph].
[29] A. Aguirre, J. Schaye, and E. Quataert, The Astrophysical Journal **561**, 550 (2001).
[30] C. M. Will, in *Theory and Experiment in Gravitational Physics* (Cambridge University Press, 2018) pp. 11–60.
[31] D. Lovelock, Journal of Mathematical Physics **12**, 498 (1971).
[32] C. M. Will, in *Theory and Experiment in Gravitational Physics* (Cambridge University Press, 2018) pp. 156–169.
[33] M. Milgrom, Physical Review D **80**, 123536 (2009).
[34] J. D. Bekenstein, Physical Review D **70**, 083509 (2004).
[35] J. W. Moffat, JCAP (2005), 10.48550/ARXIV.GR-QC/0506021.

[36] S. Boran, S. Desai, E. Kahya, and R. Woodard, Physical Review D **97**, 041501 (2018).

[37] Planck Collaboration, (2018), 10.48550/ARXIV.1807.06205.

[38] C. Skordis and T. Zlosnik, Phys. Rev. Lett. 127, 161302 (2021) (2020), 10.1103/PhysRevLett.127.161302, arXiv:2007.00082 [astro-ph.CO].

[39] B. A. Reid et al., Monthly Notices of the Royal Astronomical Society (2010), 10.1111/j.1365-2966.2010.16276.x.

[40] C. de Rham, L. Engelbrecht, L. Heisenberg, and A. Lüscher, Journal of High Energy Physics **2022** (2022), 10.1007/jhep12(2022)086.

[41] J. M. Martín-García, R. Portugal, and L. R. U. Manssur, Computer Physics Communications **177**, 640 (2007).

[42] J. Martín-García, D. Yllanes, and R. Portugal, Computer Physics Communications **179**, 586 (2008).

[43] C. Skordis and A. Durakovic, Personal communication (2023).

[44] S. M. Carroll, *Spacetime and Geometry* (Cambridge University Press, 2019).

[45] J. M. Martín-García, Computer Physics Communications **179**, 597 (2008).

[46] T. Nutma, Computer Physics Communications **185**, 1719 (2014).

[47] P. Verwayen, C. Skordis, and C. Bhm, "Aether scalar tensor (aest) theory: Quasistatic spherical solutions and their phenomenology," (2023).

Appendix A: Script for extremising the AeST action

The code compares a compact form for each of the field equations (Eqs. (20), (22) and (24)) to an expression obtained using a standard routine for variations in `xAct`, returning their difference. If the expressions match, an output of zero is expected. An example is shown for Eq. (20). The full code can be found in the file `xAct_FE_final.nb`.

```
(* Have xAct take variations w.r.t. scalar field *)
ScalarEq = VarD[Phi[], CD][LS];

(* Simplify resulting expression *)
(* Canonicalise indices *)
ScalarEq //= ToCanonical;
ScalarEq //= CollectTensors;

(* The scalar equation of Section 2B, as derived by hand *)
ExplicitFormS[a] = (2 - KB + D[Ffr[Yfr[], Qfr[]], Yfr[]]) q[a, b] CD[-b]@Phi[]
                - (2 - KB) J[a] + (1/2) D[Ffr[Yfr[], Qfr[]], Qfr[]] A[a];

(* Apply substitution routines for the definitions of Section 2A *)
ExplicitFormS[a] = ExplicitFormS[a] /. JToA;
ExplicitFormS[a] = ExplicitFormS[a] /. QfrToAPhi;
ExplicitFormS[a] = ExplicitFormS[a] /. YfrToqPhi;
ExplicitFormS[a] = ExplicitFormS[a] /. qToGA;
ScalarEqCompare = CD[-a]@ExplicitFormS[a];

(* Compare both expressions, do not suppress output *)
DifferenceS = ScalarEq - 2 ScalarEqCompare;
DifferenceS //= CollectTensors
0
```

Appendix B: Script for obtaining the spherically symmetric AeST field equations

For field components taking the values in Eqs. (45) and (46), the code prints the field equations as expressions that equal zero. A minimal example of the necessary code is given for the 0-component of Eq. (22). The full code can be found in the file `xCoba_final.nb`.

```
(* Introduce two routines for converting to spherically symmetric coordinates *)
RawSymm[Expr_] := Module[{SymmExpr = Expr},
      (* Allow simplification within scalars *)
      SymmExpr //= NoScalar;
      SymmExpr = SymmExpr /. {
      (* Subtract background from scalar field *)
       Phi[] -> Phis[cr[]] + Qvac*ct[],
       Qfr[] -> Qfrs[cr[]],
       Yfr[] -> Yfrs[cr[]]
      };
      SymmExpr //= ToBasis[SphericalPolar];
      (* Separating the metric needs to be done on the chosen basis to
      avoid placeholder indices *)
      SymmExpr //= SeparateMetric[g];
      SymmExpr //= ToBasis[SphericalPolar];
      (* Perform contractions in basis *)
      SymmExpr //= TraceBasisDummy;
      (* Substitute component values *)
      SymmExpr //= ToValues;
      (* Including in nested expressions *)
      SymmExpr //= ToValues;
      SymmExpr];

ToSymmSimple[Expr_] := Module[{SymmExpr = Expr},
      SymmExpr = SymmExpr /. {xAct`xTensor`Scalar -> RawSymm};
      SymmExpr //= RawSymm;
      (* Simplify RawSymm output *)
      SymmExpr //= Simplify;
      SymmExpr //= Normal;
      SymmExpr];

(* Now enter the field equations and expand the Section 2A notation *)
AEquations =
  KB q[b, -a] CD[-c]@F[c, -b] +
    2 (2 - KB)*(CD[b]@Phi[]) q[-a, -c] CD[c]@
      A[-b] - (2 - KB) q[-a, -b] CD[b]@
      Qfr[] - ((2 - KB + D[Ffr[Yfr[], Qfr[]], Yfr[]]) Qfr[] +
        1/2 D[Ffr[Yfr[], Qfr[]], Qfr[]] + (2 - KB) Jc[]) q[-a, -b] CD[
        b]@Phi[];
AEquations = AEquations /. JToA;
...
AEquations //= ToCanonical;

(* Separate equations for different indices *)
AEquations = AEquations // ToBasis[SphericalPolar] // ComponentArray;
(* Choose the 0-component and apply reduction routine *)
VEquationT = ToSymmSimple@(AEquations[[1]]);
(* Including on the functions Y and Q, which are evaluated in the basis elsewhere *)
VEquationT = Numerator[VEquationT /. SubstituteFreeFunctions];
(* Display equation *)
Print@VEquationT;
```

Appendix C: Spherically symmetric field equations

The full system of equations is printed in the file `xCoba_final.nb`. The 0-component of the vector equation is as follows:

$$
\begin{aligned}
&2e^{2R+T}\left(-4K_B\varphi' + 8\varphi' + R'\left(2K_B + (K_B-2)r\varphi'\right) + T'\left(2K_B + (K_B-2)r\varphi'\right) + K_B rR'' + K_B rT''\right)A^5 \\
&+ 2e^{2R}\Bigg(-4K_BQ_0\sqrt{e^T\left(e^RA^2+1\right)} + 8Q_0\sqrt{e^T\left(e^RA^2+1\right)} + K_BQ_0rR'\sqrt{e^T\left(e^RA^2+1\right)} - 2Q_0rR'\sqrt{e^T\left(e^RA^2+1\right)} \\
&+ K_BQ_0rT'\sqrt{e^T\left(e^RA^2+1\right)} - 2Q_0rT'\sqrt{e^T\left(e^RA^2+1\right)} + 4e^Tr\varphi'\left(e^{-T}Q_0\sqrt{e^T\left(e^RA^2+1\right)} + A\varphi'\right) \\
&- 2e^TK_Br\varphi'\left(e^{-T}Q_0\sqrt{e^T\left(e^RA^2+1\right)} + A\varphi'\right) + e^TA'\left(rR'K_B + rT'K_B + 2r\varphi'K_B + 4K_B - 4r\varphi'\right) + 2e^TK_BrA'' \\
&- 2e^T(K_B-2)r\left(-e^{-T}Q_0\sqrt{e^T\left(e^RA^2+1\right)}T' + \frac{e^{-T}Q_0\left(e^T\left(e^RR'A^2 + 2e^RA'A\right) + e^T\left(e^RA^2+1\right)T'\right)}{2\sqrt{e^T\left(e^RA^2+1\right)}} + A'\varphi' + A\varphi''\right) \\
&+ e^Tr\varphi'\mathscr{F}_Q + 2e^Tr\varphi'\left(e^{-T}Q_0\sqrt{e^T\left(e^RA^2+1\right)} + A\varphi'\right)\mathscr{F}_Y\Bigg)A^4 \\
&+ e^R\Bigg(e^TK_BrR'^2 + 4e^TK_BR' - e^TK_BrT'R' - 8e^Tr\varphi'R' + 4e^TK_Br\varphi'R' + 4e^R(K_B-2)Q_0r\sqrt{e^T\left(e^RA^2+1\right)}A' \\
&+ 8e^TK_BT' + 32e^T\varphi' - 16e^TK_B\varphi' - 8e^TrT'\varphi' + 4e^TK_BrT'\varphi' + 2e^TK_BrR'' + 4e^TK_BrT'' \\
&+ 2e^RQ_0r\sqrt{e^T\left(e^RA^2+1\right)}\mathscr{F}_Q - 4e^RQ_0\sqrt{e^T\left(e^RA^2+1\right)}r\left(e^{-T}Q_0\sqrt{e^T\left(e^RA^2+1\right)} + A\varphi'\right)\left(K_B - \mathscr{F}_Y - 2\right)\Bigg)A^3 \\
&+ 2e^R\Bigg(-4K_BQ_0\sqrt{e^T\left(e^RA^2+1\right)} + 8Q_0\sqrt{e^T\left(e^RA^2+1\right)} + K_BQ_0rR'\sqrt{e^T\left(e^RA^2+1\right)} - 2Q_0rR'\sqrt{e^T\left(e^RA^2+1\right)} \\
&+ K_BQ_0rT'\sqrt{e^T\left(e^RA^2+1\right)} - 2Q_0rT'\sqrt{e^T\left(e^RA^2+1\right)} + 8e^Tr\varphi'\left(e^{-T}Q_0\sqrt{e^T\left(e^RA^2+1\right)} + A\varphi'\right) \\
&- 4e^TK_Br\varphi'\left(e^{-T}Q_0\sqrt{e^T\left(e^RA^2+1\right)} + A\varphi'\right) + e^TA'\left(3rR'K_B + rT'K_B + 4r\varphi'K_B + 4K_B - 8r\varphi'\right) + 2e^TK_BrA'' \\
&- 4e^T(K_B-2)r\left(-e^{-T}Q_0\sqrt{e^T\left(e^RA^2+1\right)}T' + \frac{e^{-T}Q_0\left(e^T\left(e^RR'A^2 + 2e^RA'A\right) + e^T\left(e^RA^2+1\right)T'\right)}{2\sqrt{e^T\left(e^RA^2+1\right)}} + A'\varphi' + A\varphi''\right) \\
&+ 2e^Tr\varphi'\mathscr{F}_Q + 4e^Tr\varphi'\left(e^{-T}Q_0\sqrt{e^T\left(e^RA^2+1\right)} + A\varphi'\right)\mathscr{F}_Y\Bigg)A^2 \\
&- \Bigg(-4e^{R+T}K_BrA'^2 - 4e^R(K_B-2)Q_0r\sqrt{e^T\left(e^RA^2+1\right)}A' - 4e^TK_BT' + e^TK_BrR'T' \\
&- 16e^T\varphi' + 8e^TK_B\varphi' + 4e^TrR'\varphi' - 2e^TK_BrR'\varphi' + 4e^TrT'\varphi' - 2e^TK_BrT'\varphi' - 2e^TK_BrT'' \\
&- 2e^RQ_0\sqrt{e^T\left(e^RA^2+1\right)}r\mathscr{F}_Q + 4e^RQ_0r\sqrt{e^T\left(e^RA^2+1\right)}\left(e^{-T}Q_0\sqrt{e^T\left(e^RA^2+1\right)} + A\varphi'\right)\left(K_B - \mathscr{F}_Y - 2\right)\Bigg)A \\
&- 2e^Tr\Bigg(2(K_B-2)\left(-e^{-T}Q_0\sqrt{e^T\left(e^RA^2+1\right)}T' + \frac{e^{-T}Q_0\left(e^T\left(e^RR'A^2 + 2e^RA'A\right) + e^T\left(e^RA^2+1\right)T'\right)}{2\sqrt{e^T\left(e^RA^2+1\right)}} + A'\varphi' + A\varphi''\right) \\
&+ \varphi'\left(-2(K_B-2)A' - \mathscr{F}_Q + 2\left(e^{-T}Q_0\sqrt{e^T\left(e^RA^2+1\right)} + A\varphi'\right)\left(K_B - \mathscr{F}_Y - 2\right)\right)\Bigg) = 0.
\end{aligned}
$$

Appendix D: Analytical solution for the AeST metric components in the limit of a tensor field and vector field directed along time

The radial component of the metric is given by

$$R(r) = \mathcal{G}^{-1}\left(c_1 - 2\ln(r)\right), \tag{D1}$$

where

$$\mathcal{G}(x) = K\left(K_1 \ln\left(\sqrt{2} - X\right) + K_2 \ln(-1 + X) - K_3 \ln(1 + X) + K_4 \ln\left(\sqrt{2} + X - K_B X\right)\right),$$

using the notation

$$X = \sqrt{1 + x}, \tag{D2}$$

$$K = \left(1 + 2K_B - K_B^2\right)^{-1}, \tag{D3}$$

$$K_1 = -2\left(-1 - 2K_B + K_B^2\right), \tag{D4}$$

$$K_2 = -2 - 3\sqrt{2}K_B + \sqrt{2}K_B^2, \tag{D5}$$

$$K_3 = 2 - 3\sqrt{2}K_B + \sqrt{2}K_B^2, \tag{D6}$$

$$K_4 = 2(-1 + K_B)^2. \tag{D7}$$

Using the solution for $R(r)$, the solution for $T(r)$ can be expressed as

$$T(r) = C_1 \exp\left(\int_1^r \frac{2(-2 + \sqrt{2}\sqrt{1 + R(K_2)}}{K_2} \mathrm{d}K_2\right), \tag{D8}$$

where C_1 is an integration constant.